# High–Resolution Scanning Tunneling Microscopy Characterization of Mixed Monolayer Protected Gold Nanoparticles

**10 AUTHORS**, INCLUDING:

**Kellen Harkness**
École Polytechnique Fédérale de Lausanne
**12** PUBLICATIONS **243** CITATIONS

SEE PROFILE

**Maria Longobardi**
University of Geneva
**10** PUBLICATIONS **82** CITATIONS

SEE PROFILE

**Kunal Mali**
University of Leuven
**50** PUBLICATIONS **666** CITATIONS

SEE PROFILE

**Francesco Stellacci**
École Polytechnique Fédérale de Lausanne
**190** PUBLICATIONS **7,038** CITATIONS

SEE PROFILE

# High-Resolution Scanning Tunneling Microscopy Characterization of Mixed Monolayer Protected Gold Nanoparticles

Quy Khac Ong,[†] Javier Reguera,[†] Paulo Jacob Silva,[†] Mauro Moglianetti,[†] Kellen Harkness,[†] Maria Longobardi,[‡] Kunal S. Mali,[§] Christoph Renner,[‡] Steven De Feyter,[§] and Francesco Stellacci[†,*]

[†]Institute of Materials, École Polytechnique Fédérale de Lausanne, Lausanne, Switzerland, [‡]Department of Condensed Matter Physics, University of Geneva, Geneva, Switzerland, and [§]Department of Chemistry, Division of Molecular Imaging and Photonics, KU Leuven—University of Leuven, Celestijnenlaan 200F, 3001 Leuven, Belgium

**ABSTRACT** Gold nanoparticles protected by a binary mixture of thiolate molecules have a ligand shell that can spontaneously separate into nanoscale domains. Complex morphologies arise in such ligand shells, including striped, patchy, and Janus domains. Characterization of these morphologies remains a challenge. Scanning tunneling microscopy (STM) imaging has been one of the key approaches to determine these structures, yet the imaging of nanoparticles' surfaces faces difficulty stemming from steep surface curvature, complex molecular structures, and the possibility of imaging artifacts in the same size range. Images obtained to date have lacked molecular resolution, and only domains have been resolved. There is a clear need for images that resolve the molecular arrangement that leads to domain formation on the ligand shell of these particles. Herein we report an advance in the STM imaging of gold nanoparticles, revealing some of the molecules that constitute the domains in striped and Janus gold nanoparticles. We analyze the images to determine molecular arrangements on parts of the particles, highlight molecular "defects" present in the ligand shell, show persistence of the features across subsequent images, and observe the transition from quasi-molecular to domain resolution. The ability to resolve single molecules in the ligand shell of nanoparticles could lead to a more comprehensive understanding of the role of the ligand structure in determining the properties of mixed-monolayer-protected gold nanoparticles.
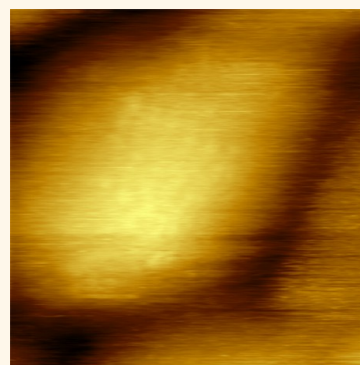
**KEYWORDS:** scanning tunneling microscopy · STM · striped nanoparticles · Janus nanoparticles · self-assembled monolayer · SAM

Monolayer-protected nanoparticles (NPs) consist of a core protected by a supramolecularly assembled ligand shell of small molecules or macro-molecules. Gold nanoparticles coated with a self-assembled monolayer (SAM) of thiolate molecules have found a large number of potential applications, ranging from drug delivery to catalysis.[1,2] The ligand shell determines a large fraction of the particles' properties. Frequently, the ligand shell is composed of multiple types of molecules, each one providing the NPs with a certain set of properties.[3,4] Sometimes properties are not simply additive, and the presence of more than one ligand type in the ligand shell imparts novel properties to the nanoparticles.[5,6] This happens because ligand molecules arrange in patches when forming the ligand shell, leading to structure-dependent properties, such as interfacial energy[5] or solubility.[7]

Weiss and co-workers used scanning tunneling microscopy (STM) to show that binary mixtures of dissimilar thiol molecules form domains when coassembling onto flat Au surfaces.[8] Some of us used STM to discover the same effect in the ligand shell of Au NPs.[9,10] On a flat surface, these domains tend to have a wide size distribution and varied shapes.[8,11−16] Once constrained on NP surfaces, these domains adopt various morphologies based on the identity of the ligands and the NP core size.[17,18] In particular, 2:1 and 1:1 mixtures of dissimilar molecules coassembled on ∼5 nm diameter Au NPs were found to form stripe-like domains with a characteristic width of ∼1 nm.[9,10]

The first reports of stripe-like domains on mixed-monolayer-protected Au NPs were

followed by in-depth STM image analysis[10] and statistical validation.[19] In a separate work, a power spectral density method to analyze these images has been developed, and it has established that identical information can be extracted from images taken in different laboratories, further confirming the validity of these images.[20] The existence of patchy ligand shell morphology has also been supported by atomic force microscopy,[5] infrared spectroscopy,[21] nuclear magnetic resonance spectroscopy,[22,23] matrix-assisted laser desorption/ionization ion mobility mass spectrometry (MALDI-IM-MS),[24] and electron spin resonance (ESR) spectroscopy.[25,26]

Glotzer and co-workers have shown through coarse-grained and molecular dynamics simulations that the stripe morphology forms because of an interplay between the enthalpy of phase separation and a conformational entropy that arises when longer molecules are at a domain boundary with shorter ones.[27,28] These conclusions were recently supported by other simulations performed on cylindrical surfaces by Glotzer[29,30] and others.[31,32]

Nanoparticles coated with striped domains have many unique structure-dependent properties that mainly derive from their interfacial interactions[5,7,33] or the presence of two polar topological defect points that can be chemically modified.[34,35] Some of these properties have led to novel applications; for example, some striped particles have been shown to spontaneously fuse with lipid bilayers[36] and penetrate cell membranes,[37−39] leading to unconventional drug delivery approaches.[40] Recently striped nanoparticles have been used as ultrasensitive and selective methyl mercury sensors.[41] It is reasonable to predict that many other properties and applications could possibly stem from the unique amphiphilic arrangements of ligand molecules on the surface of nanoparticles, which are prevalently observed in biology.

To date, experimental images and spectroscopic data on patchy particles have elucidated the presence of domains, but not the ligands arrangement that has been shown only for homoligand-protected NPs, where it has been found to have a characteristic nearest neighbor spacing of ∼0.5 nm.[42] This spacing closely resembles the spacing known to form on flat gold surfaces for the same molecules[43−45] and is consistent with what has been found for small, atomically monodisperse $Au_{102}(SC_6H_4COOH)_{44}$ clusters using single-crystal X-ray data.[46] In particular, structures of self-assembled monolayers on flat gold surfaces are extensively studied and reported.[47,48] It is known that on Au(111) octanethiols form a few superlattices (e.g., c(4×2)) stemming from the $\sqrt{3}\times\sqrt{3}$ R30° reconstruction.[47] This basic reconstruction (with a lattice spacing of 0.5 nm) is shared also by many other thiolate molecules, such as mercaptopropionic acid and mercaptoundecanol.[43,48] Shorter thiolate molecules tend to show a similar reconstruction but often have also other distorted lattices with lattice parameters that can stretch up to slightly more than 0.6 nm.[47] On other Au planes the arrangement of the molecules can change: for example, octanethiol forms a distorted hexagonal cell with $a = 0.6$ nm and $b = 0.477$ nm on Au(100).[48] Given that it has been reported that facets on thiolate ligand protected nanoparticles are mostly (111) and (100), it is reasonable to expect that self-assembled monolayers have arrangements similar to the ones described above.[49] This observation together with an understanding that curvature[10,30] and line defects[4,28] are more prominent on particles than on surfaces leads to a conclusion that for all of the molecules studied in this paper it is reasonable to expect a spacing in the monolayer in a range from 0.4 to 0.7 nm. It should be pointed out that the mechanism of SAM formation on these particles is substantially different than that of formation on flat surfaces,[24,50] with the molecules associating first to Au atoms in solution and then to the nanoparticles, thus establishing a complex interplay between the SAM structure and the gold's core structure. Here we demonstrate high-resolution imaging of mixed-monolayer-protected gold NPs. We present the first quasi-molecular resolution images of striped particles together with image analysis detailing robustness of the measurements across different laboratories and microscopes.

## RESULTS AND DISCUSSION

In this paper we imaged three types of Au NPs. The first type was coated with a mixture of 11-mercapto-1-undecanol (C11ol) and 4-mercapto-1-butanol (C4ol), hereafter called **NP1**. The second type was coated with a mixture of 1-octanethiol (C8) and mercaptopropionic acid (C$_2$COOH), hereafter called **NP2**. The third type of particles was coated only with C8, hereafter called **NP3**.

Figure 1 displays a typical STM image of the **NP1** sample, in which multiple particles showing stripe-like patterns are identifiable. Inset 1c is a digital zoom of a striped particle whose visual illustration is shown in the inset 1b. This striped structure bears features similar to those previously reported,[9,10] specifically an interstripe distance of ∼1.0 nm that does not vary significantly with scanning speeds (ranging from 0.36 to 0.92 $\mu$m/s, as illustrated by the power spectral density (PSD) analysis in Figure S1 in the Supporting Information).

Figure 2 shows a high-resolution STM image of **NP1** recorded at a bias of +100 mV and a current set point of 1.0 nA, with the highest data density available in our Bruker Multimode microscope (512 × 512 pixels). The image was acquired on the same sample used to record the image shown in Figure 1. The image is shown without processing except for a linear global plane fit. In Figure 2a the presence of brighter dots is immediately evident. On the basis of previous literature on STM of flat SAMs and of homoligand
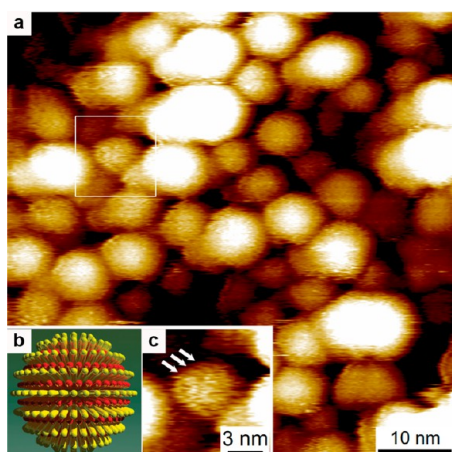
**Figure 1.** (a) Large-scale STM image of the NP1 sample. (b) Illustration of NP stripes having a molecular thickness and spacing of 1 nm. (c) Digital zoom-in of a portion of (a). The arrows are guides to the eye to identify the stripe-like domains. $I_t$ = 0.05 nA, $V_b$ = 700 mV, $S_s$ = 60.5 nm at 512 × 512 pixels. This image is part of a set of images recently taken in four different laboratories on different microscopes and by different operators.[20] A power spectral density analysis of this image is shown in Figure S1.[20]

particles,[42,43,51,52] we interpret these dots as corresponding to the tail groups (−OH) of the ligands present on **NP1**. A visual analysis of the image shows that these dots are aligned with a characteristic center-to-center spacing of ~0.5 nm along the line and ~1.0 nm between two consecutive lines, in good agreement with what is shown in Figure 1 and with previous reports.[9,10] Figure 2b shows the same image shown in Figure 2a with circles marking the dot positions. To validate our conclusions on the molecular positions, we show scan lines taken on the original image. The arrows in Figure 2b are visual aids that mark the beginning and the end of the scan lines shown in Figure 2e. A radial PSD analysis of this image (Figure 2f) shows two peaks, one at 0.83 nm and the other at 0.59 nm, confirming the visual analysis. The molecular tail groups visible as dots in this image are not the only ligands present in this sector of the NP. The density of the brighter ligand (~2 molecules/nm$^2$) is roughly half of that expected for a thiolate monolayer on a gold nanoparticle and of the one measured for these particles via thermal gravimetric analysis (TGA, ~4.5 molecules/nm$^2$, see Experimental Section), leading to the conclusion that there are other "hidden" ligands in between the ones that are visible as dots. This is expected from STM images of NPs coated with a combination of ligand molecules with a length difference of 7 methylene units.

In the same sequence of scans used to record Figure 2a, another high-resolution image of **NP1** was successfully acquired; it is shown in Figure 2c. Trace and retrace topographies and current images for these two sets of images of this particle can be found in Figures S2 and S3 in the Supporting Information.

Dots marking the tail group positions for these images show a remarkable persistence of these features. Compared to Figure 2a, a small fraction of the dots has moved slightly. It is known that thiolate molecules on gold surfaces have translational mobility[53,54] but on a time scale much longer than the acquisition time of these images; hence we rule out significant changes in molecular position. Yet STM is sensitive to molecular conformation;[55−57] hence the small variations that we observe in the images are ascribed to changes in local molecular conformation, which should to be expected given the free volume available to the molecules. Some of these conformational changes may be due to tip−sample (i.e., ligands) interactions. To extract variations in the images, we employed image difference as a tool to determine relative variations. In Figure S2d we show the difference between the trace image shown in Figure 2a and its retrace. The image is basically featureless. A similar conclusion can be reached for the image shown in Figure 2c (difference image shown in Figure S3d). In Figure 2d we show the difference between the image sets shown in Figure 2a and c (and Figures S2 and S3). Also in this case the comparison between successive images is practically featureless, showing something only in the bottom left part.

We interpret the bright dots evident in the images to correspond to the tail groups of the longer C11ol ligands. Their movement, which is expected to be perpendicular to the stripe direction (i.e., the direction with the most free volume), should hinder effective imaging of the shorter C4ol.[28] This interpretation is supported by the presence of "shadows" perpendicular to the stripes, indicating molecular movement along this direction, in good agreement with Glotzer's theory.[28] Yet, were the interpretation to be inverted (the bright dots being C4ol), nothing would change in terms of the main conclusion of this paper, which deals with the formation of separated ligand domains.

The nearest-neighbor distance of ~0.5 nm of the tail groups observed along the stripe direction is commensurate with values of intermolecular distances measured on homoligand particles[10,42] and the distance between thiolated molecules on a flat surface.[43] The suggested geometry of rows of molecules spaced ~0.5 nm along the stripe and ~1 nm perpendicular confirms the original rendition (Figure 1b) published to describe these types of particles, at least in the more ordered, central part of the imaged particle.[9] Yet, to better illustrate the structure of the molecules on these particles, we determined the coordinates of the imaged tail groups (interpreted as C11ol). We filled the "empty" space with the other molecules (C4ol) and produced a 3D rendering of the molecular arrangement on the particles that is shown in Figure S6. The image graphically represents this particle. It also illustrates that this type of high-resolution image unveils only a small part of the surface of the NP. It would be
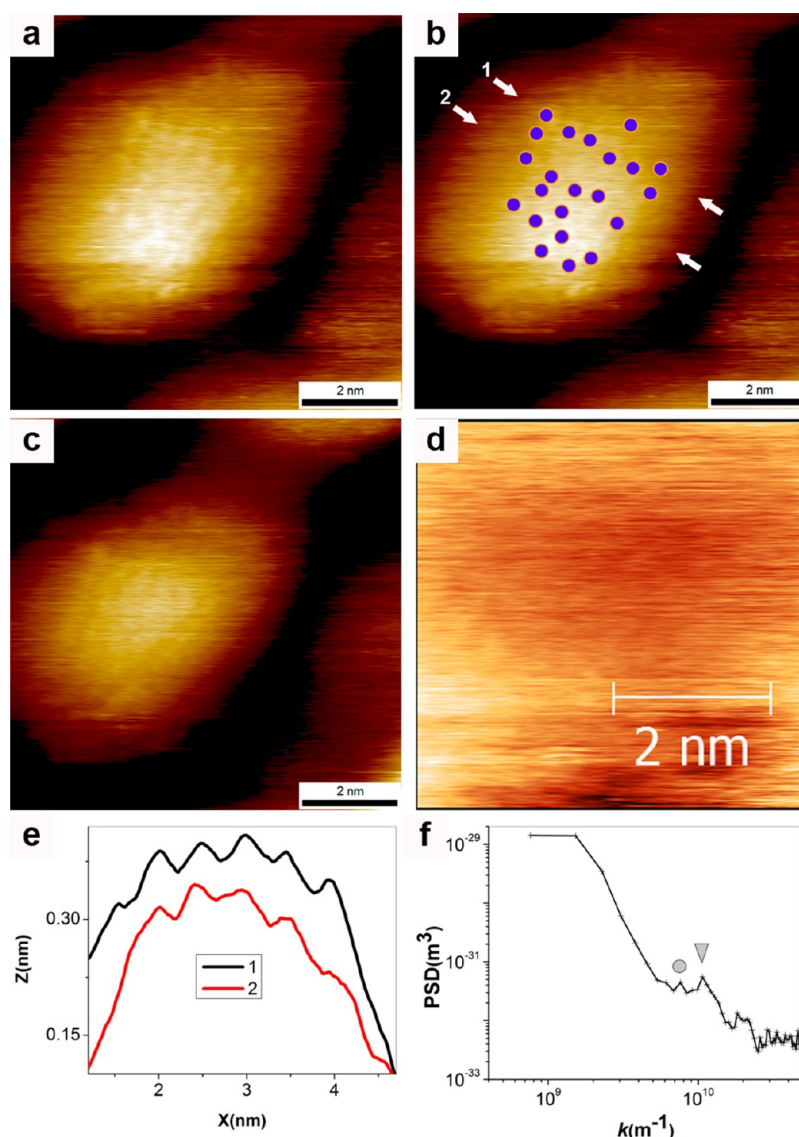
**Figure 2. High-resolution STM images of the NP1 sample. (a) As-recorded image after a first-order global plane fit. This image is the trace image of image set 1 shown completely (trace, retrace, and current) in Figure S2. (b) Image (a) with overlaid violet circles placed at the positions identified as containing bright dots. We interpret these bright dots as the tail groups of one of the two types of molecules coating the NP, probably C11ol. To extract the position of the dots in a consistent way, we employed a method currently popular in the analysis of high-resolution STM images, 2D continuous wavelet transform (CWT).[69] To the raw images we applied a 2D CWT with a Mexican hat wavelet of 14 pixels in Gwyddion.[70] The resulting images showed clear features whose position on the image was determined using the "Mark Grain" feature. An operator placed round dots on the images based on the output of this procedure. Numbers indicate profile lines shown in (e). Arrows indicate direction of the line profiles. (c) Different high-resolution image of the same particle from the same sequence of scans. This image is the trace image of image set 2 shown completely in Figure S3. (d) Image obtained as the difference between the trace plus retrace sum images of image set 1 and that of image set 2. The sum images used are shown in Figures S2e and S3e, respectively. Figure S4 shows the comparison between the sum and difference images obtained in this way. (e) Plot of the height profiles taken from image (a). Each profile is achieved by averaging height data over a stripe of thickness 14 pixels centered around the line identified by the arrows in (b). (f) Average radial PSD of the trace and retrace images from image set 1. The two symbols on the images indicate the peak at 0.83 nm (circle) and 0.59 nm (triangle) that we assign to the distance between the rows of dots and between the dots, respectively. The complete plot is shown in Figure S5. Images (a) and (c) were taken with $I_t$ = 2 nA, $V_b$ = 100 mV, $S_s$ = 8.25 nm at 512 × 512 pixels.**

reasonable to ask whether such an image can be related to the image shown in Figure 1. It is evident that the images shown in Figures 1 and 2 have markedly different quality, the former showing only domain boundaries on a number of particles and the latter showing some molecular positions but on a single particle. In both cases the spacing between

domains is ∼1 nm. In ref 20 we show that the PSD of this image obtained at this resolution can be stitched onto the PSD of images obtained at lower resolution, thus validating the use of Figure 2 to explain the molecular arrangement of the domains shown in Figure 1.[20] The high-resolution imaging of this sample has been reproduced, and representative images are
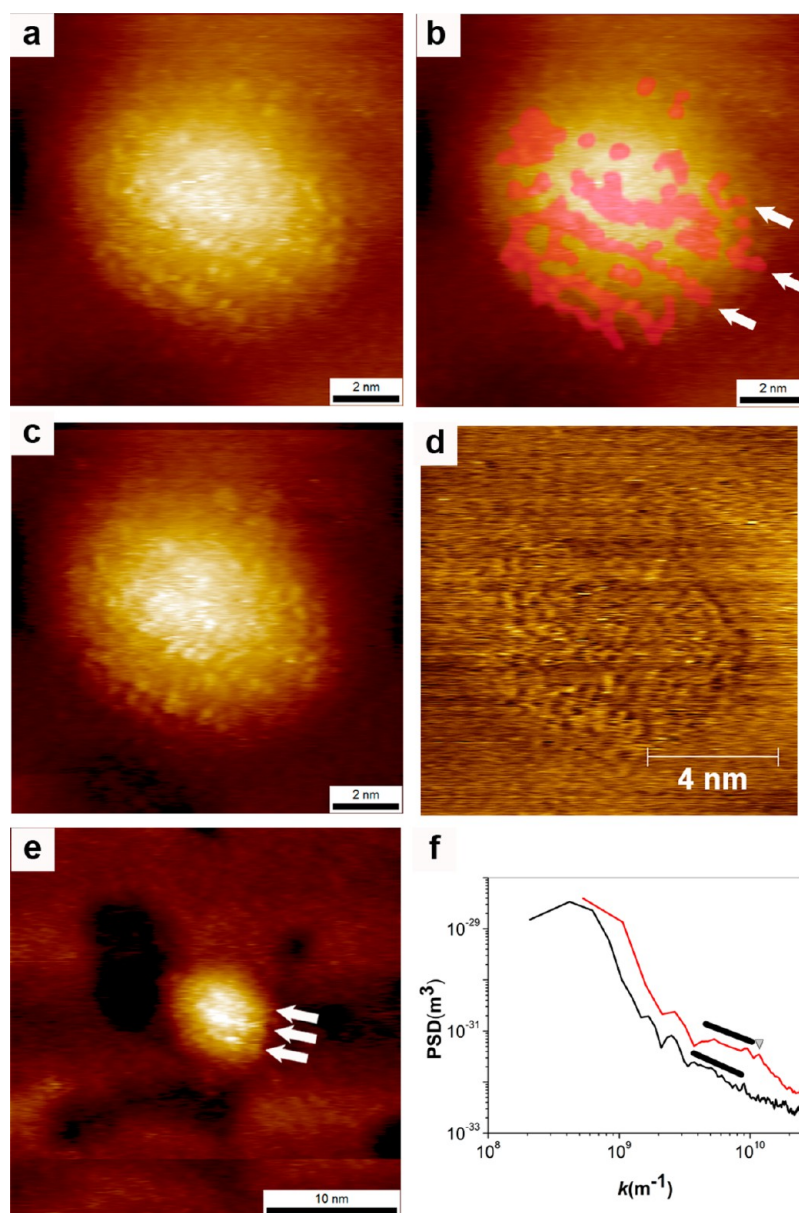
**Figure 3.** High-resolution images of the NP2 sample. Trace (a) and retrace (c) as-recorded image ($S_s$ = 11.8 nm) after a first-order global fit. Bright dots are clearly visible. These bright dots are the tail groups of one of the two types of molecules coating the NP, probably C8. (b) Image (a) with red masks overlaid onto the dots so as to evidence the continuous domain regions that these dots form. The arrows in the image are a guide to the eye indicating three parallel domains. (d) Difference image between the images shown in (a) and (c). The whole image set together with the sum image is shown in Figure S9. (e) STM topography trace image of the same particle shown in (a) taken at a lower magnification and at higher tip velocity. Arrows in this image are meant to indicate the same three stripe-like domains indicated in (b). The complete image set for this particle is shown in Figure S11. (f) Comparison between the radial PSD plots of a series of successive images of the particles shown in this figure. The red plot is the average from three images (trace and retrace) recorded at 11.8 nm scan size and 0.72 $\mu$m/s tip velocity, and the black is the average of two images (trace and retrace) recorded at 30 nm and 1.83 $\mu$m/s. The line indicates a broad peak that extends from 1.5 to 0.7 nm; this is present in both averages. The triangle is at 0.54 nm and is present only in the higher magnification images. In Figure S10 the complete plots are presented, together with average scan lines for images (a) and (e). All images were obtained with $I_t$ = 2 nA, $V_b$ = 80 mV at 512 × 512 pixels.

shown in Supporting Information Figures S7 and S8. In particular, Figure S7 is an image recorded at 77 K using a UHV LT-STM by Omicron. This image shows dots spaced 0.47 nm along the short direction and 0.86 nm along the long direction, confirming the spacing and arrangement found in Figure 2a. It is worth noticing that the image shown in Figure S7 was recorded at a much lower tip velocity compared to

the image shown in Figure 2a (0.25 and 0.018 $\mu$m/s, respectively).

We extended our high-resolution STM imaging to examine the molecular structure of stripes in another sample, **NP2**. Figure 3a is the whole image scan shown after a first-order global plane fit. Figure 3b highlights in red continuous regions containing the dots in the images to demarcate idealized domains formed by the

molecules imaged. As for **NP1** the density of these domains is roughly half the density of the ligands present on these particles determined by TGA ($\sim$4.3 molecules/nm$^2$). The shape of these "red" domains has a striking resemblance to the results of simulations published in ref 28. Figure 3c shows the retrace image whose trace is shown in Figure 3a. As observed for **NP1**, the difference between these two images (Figure 3d) is almost featureless but does show some minor roughness. The roughness does not directly correlate with the features in the images; hence we take it as an indication of minor instrumental noise present in the image that does not affect the major features.

The images shown in Figure 3 reveal a higher level of complexity (*i.e.*, information) than what has been previously seen from large-scale images. When looking closely at the dots in Figure 3a and c, it is possible to observe that stripe domains can have variable thickness, as shown in previous simulations,[28] and that multiple "point defects" are present (the red region in Figure 3b is meant to illustrate this point). In the case of **NP2** we were able to image the particle at multiple length scales and consequently tip speeds. Figure 3a and e are images of the same particle recorded at 0.72 and 1.83 $\mu$m/s, respectively. Importantly, the direct comparison between these two images leads to an observation of the transition from higher to lower resolution images of stripe-like domains. As the resolution decreases, the features comprising a stripe merge into a single continuous domain that corresponds to the stripe morphology previously observed.[9,10] In the higher resolution images, arrangements of dots in stripes similar to those on **NP1** are visible with the nearest-neighbor distance of $\sim$0.55 nm, and line profiles perpendicular to stripes indicate a spacing of $\sim$1.2 nm. In Figure 3b, arrows indicate the position of these stripes. In the lower resolution images the dots are lost and merge into elongated features that are also indicated by arrows in Figure 3e. To substantiate the claims that the domains observed in Figure 3a and e are the same, we show in Figure S10b, line profiles taken averaging over a large fraction of the particles present in these images. Both line profiles have the same shape: roughly a half-circumference with three protrusions on it. It is evident that these protrusions (the domain features in the image) align remarkably well for the scan lines of the two images. In other words, these modulations have basically the same relative position and spacing on both images, even though the imaging conditions are significantly different, and show a spacing of $\sim$1.2 nm. To quantify the spatial distribution of features on this particle in Figure 3f and S10a, we show average radial PSD plots from two sets of images (high and low magnification at 0.72 and 1.83 $\mu$m/s, respectively). In both plots a broad peak that extends from 1.5 to 0.7 nm is visible; we assign this peak to the average distance between

stripe-like domains on the particles. The high-resolution images also show a peak at 0.54 nm that we assign to the distances between the dots within the same domain (that we resolve only in these images).

There is a significant difference between the sample used to image **NP1** and the one used to image **NP2**. The former (shown in Figure 1) was composed of a dense layer of particles; the latter showed isolated particles (evident in Figure 2e). For the latter case one expects larger distortions at the particle edges and at the flat parts of the sample close to the particle due to the shape of the tip. In fact, when close to the particle edges various parts of the tip might interact with the nanoparticles instead of the flat part of the sample depending on the relative tip/particle position. In any case, we expect that these effects would be minimized when imaging the top of the particle, and this is the part of the image that we have mostly analyzed. The persistence of the features on top of the particles across many images and through different imaging conditions confirms this conclusion. The substrate onto which **NP2** was placed contained a monolayer of butanethiol and hexadecanedithiol. It is possible that parts of this mixed monolayer were also imaged, but we do not have enough evidence at the moment to make any conclusion on the images of this part of the sample.

There are a few experiments that we have performed as controls to better substantiate our assignment of the features we observe on the nanoparticles as tail groups of the ligand molecules. We rule out tip-imaging effects in the series of images that show **NP1**, as the spacing between the dots reproduces across laboratories and matches what was found in ref 20. In the case of **NP2** the spacing that we observe is the same spacing reported for these types of particles in the past in ref 19. We believe that we image molecular features and not features related to the gold core, as high-resolution transmission electron microscopy images of these particles do not show any evidence of protrusions with these spacings (see Figure S12). Additionally, we performed a series of imaging for a nanoparticle sample by changing the set current. We first found imaging conditions that allowed the observation of clear features on the nanoparticles. We interpret these features as due to imaging of molecules on the particles. To prove this point, we changed the imaging set current to force the tip inside the ligand shell. As expected, the features disappeared, smooth nanoparticle surfaces were imaged, and hints of facets could be seen (see Figure S13 in the Supporting Information). When the imaging set current was reset to the original value (and consequently the tip was lifted above the ligand shell), the features on the nanoparticles reappeared. This control experiment shows (i) that our images have features that are due to the molecules in the ligand shell, (ii) that the features
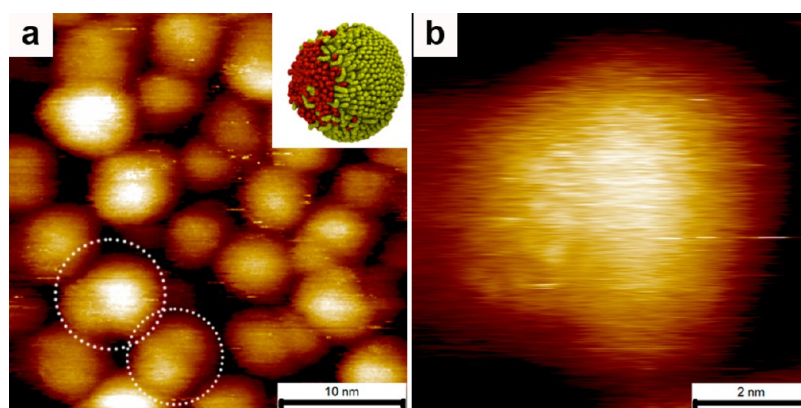
**Figure 4. High-resolution STM image of the NP1 sample. (a) Large-scale image ($S_s$ = 32.6 nm, $I_t$ = 30 pA, $V_b$ =700 mV). Dashed white circles indicate the presence of Janus particles. A cartoon of the Janus structure is illustrated in the inset. (b) High-resolution image of a Janus particle taken with $I_t$ = 2 nA, $V_b$ = 500 mV at 512 × 512 pixels.**

imaged are on the nanoparticles and not on the tip, and finally (iii) that the feedback conditions used were properly set, with no feedback instability. We are also confident in the ability of discerning different molecular arrangements on nanoparticles, as on the same **NP1** sample used to record Figures 1 and 2 we were able to identify particles composed of two separate domains (*i.e.*, Janus particle). Indeed, we have recently discovered that certain molecular combinations of ligand molecules lead to a spontaneous formation of Janus particles.[18] For **NP1** particles, the stripe morphology dominates, but there are also Janus particles. Figure 4a is a large-scale image of the same **NP1** sample shown in Figures 1 and 2. In this region, NPs with Janus structures are highlighted by dashed circles. Each Janus particle possesses two hemispherical domains demarcated by a boundary line. Molecular resolution STM imaging also identifies some molecular details of these particles. A high-resolution image is presented in Figure 4b, showing a region on the left of the particle in which discrete molecular tail groups are visible. Additional images of Janus particles are shown in Figure S14. While a discussion on Janus NPs and their images does not pertain to this paper, the main point of the images shown in Figure 4 is to show that the sample imaged in Figures 1 and 2 contains particles with a substantially different morphology from the one shown in those figures.

Finally, to further test the correlation between the features we image in STM and the ligand shell composition, we synthesized homoligand nanoparticles (**NP3**) and studied them. Figures 5 and S15 show an image of C8-coated NPs. Dots resembling the ones present on the particle shown in Figure 2a are clearly evident. In Figure 5b these dots are highlighted by superimposed violet circles, placed using the same procedure used to place the same circles in Figure 2b. There are clear qualitative differences between the arrangement of the dots (and consequently the circles) in the images of **NP1** (Figure 2) and **NP3** (Figure 5).

While for mixed ligand particles alignment is clear with a compact arrangement of these dots along one direction and a looser one along the perpendicular direction, this is not true for homoligand particles, where a more isotropic distribution of these dots is evident. The radial PSD shown in Figure 5f shows a broad feature from 0.9 to 0.63 nm with two peaks at the extremes corresponding to the distribution of distances that we observe in the image. It is worth noticing that compared to the images shown in Figures 2 and 3 the contrast of the dots that are in Figure 5 is significantly less. This is in good agreement with the composition of the NPs, as in the case of **NP3** all ligands have the same length (and very similar STM contrast), as opposed to **NP1** and **NP2**, where the difference in length (and STM contrast) between the two molecules creates better STM imaging conditions. Finally we can preliminarily state that on **NP3** we observe a disordered arrangement of the ligands. This observation is in good agreement with molecular dynamics calculations;[58−60] yet it is evident for the images in Figure 5 that probably we do not image all of the ligands. Hence further work will be required to better address this point. In the case of **NP3** the density of the ligands observed is, at least locally, close to the one measured via TGA (∼5 molecules/nm²).

Despite our efforts, the current understanding of STM imaging of mixed-SAM-coated nanoparticles is far from complete.[42,61] In particular, given that these images are of a sample with highly curved surfaces; it is reasonable to ask whether there is a need for a correction of the distances reported here. This correction could entail the elimination of drift[43] and curvature.[62,63] The former should not be necessary, as this resolution is only possible when drift is small. As for the latter, this is a complex matter that requires knowledge of the true tip trajectory. It is known that when imaging in constant height mode, curved surfaces are projected radially onto the flat tip path; consequently, distances in STM images are larger than the real ones, with the distortions being larger at the edges of the curved features.[62,63] We obtain
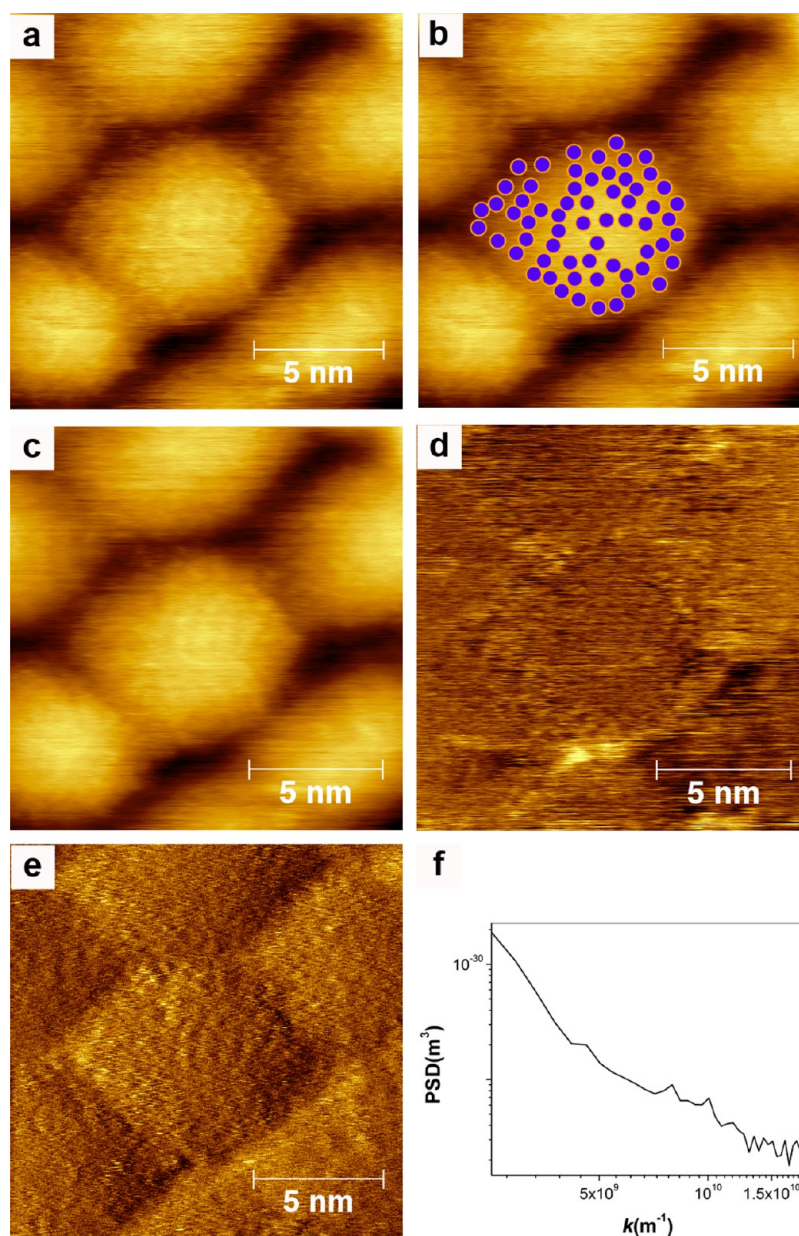
**Figure 5. High-resolution STM images of the NP3 sample. (a) As-recorded image after a second-order global plane fit. This image is the retrace image of an image set shown completely (trace, retrace, and current) in Figure S15. (b) Image (a) with overlaid violet circles placed at the positions identified as containing bright dots in (a). The dot positions were extracted in the same way described in the caption of Figure 2, the only difference being that the size of the Mexican hat wavelet was chosen to be 12 pixels. (c) Image obtained as the sum between the trace and retrace images of this set. (d) Image obtained as the difference image between the trace and retrace image. (e) Current image of this set. (f) Radial PSD of the retrace image shown in (a) (full scale of this plot is shown in Figure S15). This set of images was acquired with $I_t$ = 0.35 nA, $V_b$ = 1000 mV, and $S_s$ = 15 nm at 512 × 512 pixels.**

images in a quasi-constant current mode; hence our tip path is curved. However, the same physics applies here, and hence there is a degree of distance stretching to be expected. The curved tip path is also projected orthographically onto a flat line by the imaging software, thus leading to a shrinking of the distances. These effects are obviously opposed to each other, and they both need to be mediated by the well-known tip convolution problems. All three effects are larger on steep surfaces (*i.e.*, at the edges of the particles). The interplay between these three effects depends strictly on the trajectory of the tip;

each one can dominate depending on the specific case. Figure S16 is an attempt at a representation of these effects for a reasonably drawn trajectory,[64] showing that the effect leads to spacings that are very close to the real ones. A deeper attempt to address this issue was achieved through the generation of a 3D model of our particles. In Figure S17 we show a 3D rendering of particles consistent in shape with the findings in this paper. This image was then converted into a 3D map with the height being a gray scale map. To this latter image we applied a ball-rolling filter to capture both the

stretching and the convolution effect discussed above (Figure S17b and c) and then took a line scan of the produced image to capture the orthographic projection issue. The result is shown in Figure S17d overlapped with an experimental line scan taken from Figure 3a. There is a good agreement of the two line scans. In the case of the simulated line scan, where the initial distance was imposed and consequently is known, we can state with certainty that we find minimal size distortion in the final profile.

More simplistically, it is evident that the spacings shown in this paper for close-packed tail groups are very close to the ones measured in SAMs on flat surfaces; hence we do not expect large distortions of the images. Yet it should be pointed out that the spacing measured on flat gold surfaces is specific to Au(111) facets. On nanoparticles one expects a variety of faces, with the (111) being prevalent; hence a variation in faceting of the NPs has to be considered as another possible cause of variation in tail-group spacing. We have tried to address the issue of facets in the images of our particles by analyzing in-depth the STM images presented. We have attempted to determine the gold core shape by digitally removing the ligand-related features from the images and then allowing the STM image analysis software to find the most probable surface "background". A close inspection of the image in Figure 2 shows a flat central region with a polygonal shape (see Figure S18). Figure S19 shows the most probable crystal structure for the particles shown in Figures 3 and 5. The latter has a core particle of clear pentatwinned shape. Figure S20 overlays the molecular positions illustrated in Figures 2, 3, and 5 with the facets that we believe are most probable on the gold core. It is immediately evident that little correlation can be found between molecular arrangement and core facets. Hence, this preliminary analysis seems to rule out a major effect of the crystal structure of the gold core on the ligand shell arrangement. Larger image sets will need to be analyzed in order to reach final conclusions on this problem.

## CONCLUSIONS

In conclusion we have shown here the first images of mixed-ligand-protected nanoparticles where molecules forming stripe-like domains are visualized in both C4ol:C11ol and C8:C2COOH NPs. We believe that the approach presented here enables a better characterization of the patchiness on nanoparticles and could in the future allow for the extraction of information about the local variation of patch spacing as well as molecular defects present in the ligand shell of nanoparticles. There are a multitude of ligand-shell structures that could be determined experimentally with an appropriate high-resolution imaging capability.[65−67]

## EXPERIMENTAL SECTION

The NPs used in this paper were synthesized by a modification of the method described by Zheng et al.[68] and characterized by transmission electron microscopy (TEM) and $^1$H NMR before and after decomposition with potassium cyanide (see Supporting Information for details). NPs were thoroughly cleaned using centrifugation as described in Supporting Information. The resulting NPs were deposited on a gold(111)/mica surface by a Langmuir−Shaefer technique (see Supporting Information). At the Ecole Polytechnique Fédérale de Lausanne (EPFL), we used a Bruker Multimode Nanoscope IIIA, equipped with an E-scanner, to image the particle surface structures. At KU Leuven, we used a Bruker Multimode Nanoscope IIIA, equipped with an A-scanner. At the University of Geneva, an Omicron LT-STM at 77 K was used. All images shown in the main text of the paper were acquired at EPFL with the exception of the image shown in Figure 1, which was acquired in Leuven. In the Supporting Information all images shown were recorded at EPFL unless otherwise indicated. Typical range of current set points ($I_t$) is from 50 to 2000 pA and bias voltage ($V_b$) from 100 to 1000 mV, with precise values including the scan size ($S_s$) and pixel density provided in each figure caption. Microscopes were calibrated occasionally with a gold(111) surface and highly oriented pyrolitic graphite (HOPG).

A number of precautions were taken in order to enhance resolution, accuracy, and reproducibility of the data. To prevent STM tip contamination, the particles were cleaned several times with solvents to remove excess ligand molecules, and solution $^1$H NMR was performed to ensure a minimal presence of free ligands. To achieve the high resolution shown here, for the room-temperature imaging, it was necessary for thermal drift to be minimized by allowing the STM tip to scan on a small area (~100 nm$^2$) of the sample for a period of hours. It is noted that the need for thermal equilibration is more stringent for NP imaging when compared to the imaging of highly crystalline samples (i.e., HOPG) because they contain only short-range order, and hence drift tends to merge features in a way that is difficult to predict and interpret. To avoid imaging particles modified by the tip, images were subsequently acquired on a different part of the sample. Finally, to minimize the effects of molecular movements during imaging, images had to be acquired at sufficiently high speed (0.2−0.7 $\mu$m/s).

## REFERENCES AND NOTES

1. Daniel, M. C.; Astruc, D. Gold Nanoparticles: Assembly, Supramolecular Chemistry, Quantum-Size-Related Properties, and Applications toward Biology, Catalysis, and Nanotechnology. *Chem. Rev.* **2004**, *104*, 293–346.

2. Pelaz, B.; Jaber, S.; de Aberasturi, D. J.; Wulf, V.; Aida, T.; de la Fuente, J. M.; Feldmann, J.; Gaub, H. E.; Josephson, L.; Kagan, C. R.; *et al.* The State of Nanoparticle-Based Nanoscience and Biotechnology: Progress, Promises, and Challenges. *ACS Nano* **2012**, *6*, 8468–8483.

3. Medintz, I. L.; Uyeda, H. T.; Goldman, E. R.; Mattoussi, H. Quantum Dot Bioconjugates For Imaging, Labelling and Sensing. *Nat. Mater.* **2005**, *4*, 435–446.

4. Ingram, R. S.; Hostetler, M. J.; Murray, R. W. Poly-Hetero-$\omega$-Functionalized Alkanethiolate-Stabilized Gold Cluster Compounds. *J. Am. Chem. Soc.* **1997**, *119*, 9175–9178.

5. Kuna, J. J.; Voitchovsky, K.; Singh, C.; Jiang, H.; Mwenifumbo, S.; Ghorai, P. K.; Stevens, M. M.; Glotzer, S. C.; Stellacci, F. The Effect of Nanometre-Scale Structure on Interfacial Energy. *Nat. Mater.* **2009**, *8*, 837–842.

6. Milette, J.; Toader, V.; Reven, L.; Lennox, R. B. Tuning the Miscibility of Gold Nanoparticles Dispersed in Liquid Crystals *via* the Thiol-for-DMAP Reaction. *J. Mater. Chem.* **2011**, *21*, 9043–9050.

7. Centrone, A.; Penzo, E.; Sharma, M.; Myerson, J. W.; Jackson, A. M.; Marzari, N.; Stellacci, F. The Role of Nanostructure in the Wetting Behavior of Mixed-Monolayer-Protected Metal Nanoparticles. *Proc. Natl. Acad. Sci. U.S.A.* **2008**, *105*, 9886–9891.

8. Stranick, S. J.; Atre, S. V.; Parikh, A. N.; Wood, M. C.; Allara, D. L.; Winograd, N.; Weiss, P. S. Nanometer-Scale Phase Separation in Mixed Composition Self-Assembled Monolayers. *Nanotechnology* **1996**, *7*, 438–442.

9. Jackson, A. M.; Myerson, J. W.; Stellacci, F. Spontaneous Assembly of Subnanometre-Ordered Domains in the Ligand Shell of Monolayer-Protected Nanoparticles. *Nat. Mater.* **2004**, *3*, 330–336.

10. Jackson, A. M.; Hu, Y.; Silva, P. J.; Stellacci, F. From Homoligand- to Mixed-Ligand-Monolayer-Protected Metal Nanoparticles: A Scanning Tunneling Microscopy Investigation. *J. Am. Chem. Soc.* **2006**, *128*, 11135–11149.

11. Stranick, S. J.; Kamna, M. M.; Krom, K. R.; Parikh, A. N.; Allara, D. L.; Weiss, P. S. Scanning Tunneling Microscopy Studies of Self-Assembled Monolayers of Alkanethiols on Gold. *J. Vac. Sci. Technol., B* **1994**, *12*, 2004–2007.

12. Anderson, M. E.; Smith, R. K.; Donhauser, Z. J.; Hatzor, A.; Lewis, P. A.; Tan, L. P.; Tanaka, H.; Horn, M. W.; Weiss, P. S. Exploiting Intermolecular Interactions and Self-Assembly for Ultrahigh Resolution Nanolithography. *J. Vac. Sci. Technol. B* **2002**, *20*, 2739–2744.

13. Stranick, S. J.; Parikh, A. N.; Tao, Y. T.; Allara, D. L.; Weiss, P. S. Phase Separation of Mixed-Composition Self-Assembled Monolayers into Nanometer Scale Molecular Domains. *J. Phys. Chem.* **1994**, *98*, 7636–7646.

14. Atre, S. V.; Liedberg, B.; Allara, D. L. Chain Length Dependence of the Structure and Wetting Properties in Binary Composition Monolayers of OH- and $CH_3$-Terminated Alkanethiolates on Gold. *Langmuir* **1995**, *11*, 3882–3893.

15. Tamada, K.; Hara, M.; Sasabe, H.; Knoll, W. Surface Phase Behavior of n-Alkanethiol Self-Assembled Monolayers Adsorbed on Au(111): An Atomic Force Microscope Study. *Langmuir* **1997**, *13*, 1558–1566.

16. Hayes, W. A.; Kim, H.; Yue, X.; Perry, S. S.; Shannon, C. Nanometer-Scale Patterning of Surfaces Using Self-Assembly Chemistry. 2. Preparation, Characterization, and Electrochemical Behavior of Two-Component Organothiol Monolayers on Gold Surfaces. *Langmuir* **1997**, *13*, 2511–2518.

17. Carney, R. P.; DeVries, G. A.; Dubois, C.; Kim, H.; Kim, J. Y.; Singh, C.; Ghorai, P. K.; Tracy, J. B.; Stiles, R. L.; Murray, R. W.; *et al.* Size Limitations for the Formation of Ordered Striped Nanoparticles. *J. Am. Chem. Soc.* **2008**, *130*, 788–799.

18. Reguera, J.; Ong, Q.; Pons-Sieperman, I. C.; Yu, M.; Glotzer, S. C.; Stellacci, F. Janus Nanoparticles via Spontaneous Separation in Mixed Self-Assembled Monolayers of Alkane-Thiols, submitted.

19. Hu, Y.; Wunsch, B. H.; Sahni, S.; Stellacci, F. Statistical Analysis of Scanning Tunneling Microscopy Images of 'Striped' Mixed Monolayer Protected Gold Nanoparticles. *J. Scanning Probe Microsc.* **2009**, *4*, 24–35.

20. Biscarini, F.; Ong, Q.; Albonetti, C.; Longobardi, M.; Mali, K. S.; Ciesielski, A.; Reguera, J.; Renner, C.; Feyter, S.; Samorì, P.; *et al.* Quantitative Analysis of Scanning Tunneling Microscopy Images of Functionalized Nanoparticles, submitted.

21. Centrone, A.; Hu, Y.; Jackson, A. M.; Zerbi, G.; Stellacci, F. Phase Separation on Mixed-Monolayer-Protected Metal Nanoparticles: A Study by Infrared Spectroscopy and Scanning Tunneling Microscopy. *Small* **2007**, *3*, 814–817.

22. Liu, X.; Yu, M.; Kim, H.; Mameli, M.; Stellacci, F. Determination of Monolayer-Protected Gold Nanoparticle Ligand-Shell Morphology Using NMR. *Nat. Commun.* **2012**, *3*, 1182.

23. Guarino, G.; Rastrelli, F.; Scrimin, P.; Mancin, F. Lanthanide-Based NMR: A Tool to Investigate Component Distribution in Mixed-Monolayer-Protected Nanoparticles. *J. Am. Chem. Soc.* **2012**, *134*, 7200–7203.

24. Harkness, K. M.; Balinski, A.; McLean, J. A.; Cliffel, D. E. Nanoscale Phase Segregation of Mixed Thiolates on Gold Nanoparticles. *Angew. Chem., Int. Ed.* **2011**, *50*, 10554–10559.

25. Gentilini, C.; Franchi, P.; Mileo, E.; Polizzi, S.; Lucarini, M.; Pasquato, L. Formation of Patches on 3D SAMs Driven by Thiols with Immiscible Chains Observed by ESR Spectroscopy. *Angew. Chem., Int. Ed.* **2009**, *48*, 3060–3064.

26. Lucarini, M.; Pasquato, L. ESR Spectroscopy as a Tool to Investigate the Properties of Self-Assembled Monolayers Mrotecting Gold Nanoparticles. *Nanoscale* **2010**, *2*, 668–676.

27. Glotzer, S. C.; Solomon, M. J. Anisotropy of Building Blocks and Their Assembly Into Complex Structures. *Nat. Mater.* **2007**, *6*, 557–562.

28. Singh, C.; Ghorai, P. K.; Horsch, M. A.; Jackson, A. M.; Larson, R. G.; Stellacci, F.; Glotzer, S. C. Entropy-Mediated Patterning of Surfactant-Coated Nanoparticles and Surfaces. *Phys. Rev. Lett.* **2007**, 99.

29. Singh, C.; Hu, Y.; Khanal, B. P.; Zubarev, E. R.; Stellacci, F.; Glotzer, S. C. Striped Nanowires and Nanorods from Mixed SAMS. *Nanoscale* **2011**, *3*, 3244–3250.

30. Ghorai, P. K.; Glotzer, S. C. Atomistic Simulation Study of Striped Phase Separation in Mixed-Ligand Self-Assembled Monolayer Coated Nanoparticles. *J. Phys. Chem. C* **2010**, *114*, 19182–19187.

31. Miller, W. L.; Bozorgui, B.; Klymko, K.; Cacciuto, A. Free Energy of Alternating Two-Component Polymer Brushes on Cylindrical Templates. *J. Chem. Phys.* **2011**, *135*, 244902–5.

32. Egorov, S. A. Microphase Separation of Mixed Polymer Brushes Physisorbed on Cylindrical Surfaces. *Soft Matter* **2012**, *8*, 3971–3979.

33. Uzun, O.; Hu, Y.; Verma, A.; Chen, S.; Centrone, A.; Stellacci, F. Water-Soluble Amphiphilic Gold Nanoparticles with Structured Ligand Shells. *Chem. Commun.* **2008**, 196–198.

34. DeVries, G. A.; Brunnbauer, M.; Hu, Y.; Jackson, A. M.; Long, B.; Neltner, B. T.; Uzun, O.; Wunsch, B. H.; Stellacci, F. Divalent Metal Nanoparticles. *Science* **2007**, *315*, 358–361.

35. Nakata, K.; Hu, Y.; Uzun, O.; Bakr, O.; Stellacci, F. Chains of Superparamagnetic Nanoparticles. *Adv. Mater.* **2008**, *20*, 4294–4299.

36. Carney, R. P.; Astier, Y.; Carney, T. M.; Voïtchovsky, K.; Jacob Silva, P. H.; Stellacci, F. Electrical Method to Quantify Nanoparticle Interaction with Lipid Bilayers. *ACS Nano* **2012**, *7*, 932–942.

37. Verma, A.; Uzun, O.; Hu, Y. H.; Hu, Y.; Han, H. S.; Watson, N.; Chen, S. L.; Irvine, D. J.; Stellacci, F. Surface-Structure-Regulated Cell-Membrane Penetration by Monolayer-Protected Nanoparticles. *Nat. Mater.* **2008**, *7*, 588–595.

38. Carney, R.; Carney, T.; Mueller, M.; Stellacci, F. Dynamic Cellular Uptake of Mixed-Monolayer Protected Nanoparticles. *Biointerphases* **2012**, *7*, 1–9.

39. Leduc, C.; Jung, J.-M.; Carney, R. R.; Stellacci, F.; Lounis, B. Direct Investigation of Intracellular Presence of Gold Nanoparticles via Photothermal Heterodyne Imaging. *ACS Nano* **2011**, *5*, 2587–2592.

40. Jewell, C. M.; Jung, J.-M.; Atukorale, P. U.; Carney, R. P.; Stellacci, F.; Irvine, D. J. Oligonucleotide Delivery by Cell-Penetrating "Striped" Nanoparticles. *Angew. Chem., Int. Ed.* **2011**, *50*, 12312–12315.

41. Cho, E. S.; Kim, J.; Tejerina, B.; Hermans, T. M.; Jiang, H.; Nakanishi, H.; Yu, M.; Patashinski, A. Z.; Glotzer, S. C.; *et al.* Ultrasensitive Detection of Toxic Cations through Changes in the Tunnelling Current across Films of Striped Nanoparticles. *Nat. Mater.* **2012**, *11*, 978–985.

42. Yu, M.; Stellacci, F. Response to "Stripy Nanoparticles Revisited". *Small* **2012**, *8*, 3720–3726.

43. Dubois, C.; Stellacci, F. Self-assembled Monolayer of Short Carboxyl-Terminated Molecules Investigated with *ex Situ* Scanning Tunneling Microscopy. *J. Phys. Chem. C* **2008**, *112*, 7431–7435.

44. Ulman, A. Formation and Structure of Self-Assembled Monolayers. *Chem. Rev.* **1996**, *96*, 1533–1554.

45. Poirier, G. E. Characterization of Organosulfur Molecular Monolayers on Au(111) Using Scanning Tunneling Microscopy. *Chem. Rev.* **1997**, *97*, 1117–1128.

46. Jadzinsky, P. D.; Calero, G.; Ackerson, C. J.; Bushnell, D. A.; Kornberg, R. D. Structure of a Thiol Monolayer-Protected Gold Nanoparticle at 1.1 Å Resolution. *Science* **2007**, *318*, 430–433.

47. Vericat, C.; Vela, M. E.; Benitez, G.; Carro, P.; Salvarezza, R. C. Self-Assembled Monolayers of Thiols and Dithiols on Gold: New Challenges for a Well-Known System. *Chem. Soc. Rev.* **2010**, *39*, 1805–1834.

48. Schreiber, F. Structure and Growth of Self-Assembling Monolayers. *Prog. Surf. Sci.* **2000**, *65*, 151–257.

49. Azcárate, J. C.; Corthey, G.; Pensa, E.; Vericat, C.; Fonticelli, M. H.; Salvarezza, R. C.; Carro, P. Understanding the Surface Chemistry of Thiolate-Protected Metallic Nanoparticles. *J. Phys. Chem. Lett.* **2013**, 3127–3138.

50. Li, Y.; Zaluzhna, O.; Xu, B.; Gao, Y.; Modest, J. M.; Tong, Y. J. Mechanistic Insights into the Brust−Schiffrin Two-Phase Synthesis of Organo-Chalcogenate-Protected Metal Nanoparticles. *J. Am. Chem. Soc.* **2011**, *133*, 2092–2095.

51. Han, P.; Kurland, A. R.; Giordano, A. N.; Nanayakkara, S. U.; Blake, M. M.; Pochas, C. M.; Weiss, P. S. Heads and Tails: Simultaneous Exposed and Buried Interface Imaging of Monolayers. *ACS Nano* **2009**, *3*, 3115–3121.

52. Bumm, L. A.; Arnold, J. J.; Charles, L. F.; Dunbar, T. D.; Allara, D. L.; Weiss, P. S. Directed Self-Assembly to Create Molecular Terraces with Molecularly Sharp Boundaries in Organic Monolayers. *J. Am. Chem. Soc.* **1999**, *121*, 8017–8021.

53. Rapino, S.; Zerbetto, F. Dynamics of Thiolate Chains on a Gold Nanoparticle. *Small* **2007**, *3*, 386–388.

54. Ionita, P.; Volkov, A.; Jeschke, G.; Chechik, V. Lateral Diffusion of Thiol Ligands on the Surface of Au Nanoparticles: An Electron Paramagnetic Resonance Study. *Anal. Chem.* **2007**, *80*, 95–106.

55. Bucher, J. P.; Santesson, L.; Kern, K. Selective Imaging of Self-Assembled Monolayers by Tunneling Microscopy. *Appl. Phys. A: Mater. Sci. Process.* **1994**, *59*, 135–138.

56. Azzam, W.; Cyganik, P.; Witte, G.; Buck, M.; Wöll, C. Pronounced Odd-Even Changes in the Molecular Arrangement and Packing Density of Biphenyl-Based Thiol SAMs: A Combined STM and LEED Study. *Langmuir* **2003**, *19*, 8262–8270.

57. Poirier, G. E.; Tarlov, M. J.; Rushmeier, H. E. Two-Dimensional Liquid Phase and the $p \times \sqrt{3}$ Phase of Alkanethiol Self-Assembled Monolayers on Au(111). *Langmuir* **1994**, *10*, 3383–3386.

58. Ghorai, P. K.; Glotzer, S. C. Molecular Dynamics Simulation Study of Self-Assembled Monolayers of Alkanethiol Surfactants on Spherical Gold Nanoparticles. *J. Phys. Chem. C* **2007**, *111*, 15857–15862.

59. Luedtke, W. D.; Landman, U. Structure and Thermodynamics of Self-Assembled Monolayers on Gold Nanocrystallites. *J. Phys. Chem. B* **1998**, *102*, 6566–6572.

60. Lane, J. M. D.; Grest, G. S. Spontaneous Asymmetry of Coated Spherical Nanoparticles in Solution and at Liquid-Vapor Interfaces. *Phys. Rev. Lett.* **2010**, *104*, 235501.

61. Cesbron, Y.; Shaw, C. P.; Birchall, J. P.; Free, P.; Levy, R. Stripy Nanoparticles Revisited. *Small* **2012**, *8*, 3714–3719.

62. Meunier, V.; Lambin, P. Tight-Binding Computation of the STM Image of Carbon Nanotubes. *Phys. Rev. Lett.* **1998**, *81*, 5588–5591.

63. Venema, L.; Meunier, V.; Lambin, P.; Dekker, C. Atomic Structure of Carbon Nanotubes from Scanning Tunneling Microscopy. *Phys. Rev. B* **2000**, *61*, 2991–2996.

64. Klyachko, D.; Chen, D. M. Cluster Shapes in STM Images of Isolate Clusters and Cluster Materials. *Surf. Sci.* **2000**, *446*, 98–102.

65. Pons-Siepermann, I. C.; Glotzer, S. C. Design of Patchy Particles Using Quaternary Self-Assembled Monolayers. *ACS Nano* **2012**, *6*, 3919–3924.

66. Pons-Siepermann, I. C.; Glotzer, S. C. Design of Patchy Particles Using Ternary Self-Assembled Monolayers. *Soft Matter* **2012**, *8*, 6226–6231.

67. Santos, A.; Millan, J. A.; Glotzer, S. C. Facetted Patchy Particles through Entropy-Driven Patterning of Mixed Ligand SAMS. *Nanoscale* **2012**, *4*, 2640–2650.

68. Zheng, N.; Fan, J.; Stucky, G. D. One-Step One-Phase Synthesis of Monodisperse Noble-Metallic Nanoparticles and Their Colloidal Crystals. *J. Am. Chem. Soc.* **2006**, *128*, 6550–6551.

69. Gackenheimer, C.; Cayon, L.; Reifenberger, R. Analysis of Scanning Probe Microscope Images Using Wavelets. *Ultramicroscopy* **2006**, *106*, 389–397.

70. Nečas, D.; Klapetek, P. Gwyddion: An Open-Source Software for SPM Data Analysis. *Cent. Eur. J. Phys.* **2012**, *10*, 181–188.